ChemComm

Cite this: *Chem. Commun.*, 2011, **47**, 2747–2762

www.rsc.org/chemcomm

FEATURE ARTICLE

STM studies of single molecules: molecular orbital aspects

Bin Li, Zhenyu Li, Jinlong Yang* and J. G. Hou*

Received 4th August 2010, Accepted 13th December 2010
DOI: 10.1039/c0cc03021j

As a fundamental and frequently referred concept in modern chemistry, the molecular orbital plays a vital role in the science of single molecules, which has become an active field in recent years. For the study of single molecules, scanning tunneling microscopy (STM) has been proven to be a powerful scientific technique. Utilizing specific distribution of the molecular orbitals at spatial, energy, and spin scales, STM can explore many properties of single molecule systems, such as geometrical configuration, electronic structure, magnetic polarization, and so on. Various interactions between the substrate and adsorbed molecules are also understood in terms of the molecular orbitals. Molecular engineering methods, such as mode-selective chemistry based on the molecular orbitals, and resonance tunneling between the molecular orbitals of the molecular sample and STM tip, have stimulated new advances of single molecule science.

1. Introduction

The molecule, defined as a sufficiently stable group of atoms held by strong chemical bonds between them, is a fundamental research object of chemistry and related fields. Single molecules have discrete and abundant electronic states, which can be modified by changing their functional groups. They participate in various physical and chemical procedures, and can also be used as important components in designing functional devices at the nano-scale.[1–7] A vital concept of the single molecule is the molecular orbital, which originates from the mean field theory of quantum chemistry. Together with the concept of chemical bonds, the molecular orbital has been successfully applied to interpret properties of various chemical objects and related phenomena. Qualitatively, the ground-state property of single molecules can be fully described by an assembly of the molecular orbitals. Therefore, investigation of the molecular orbitals is key to exploring the field of single molecule science.[8–13]

During the past three decades, scanning probe microscopies, especially the well-known scanning tunneling microscopy (STM), have thoroughly changed the way of exploring the nano-world by using their abilities of directly "seeing" and "moving" atoms and individual molecules. The STM was invented in 1981 by Binnig *et al.* at IBM Zurich research

Hefei National Laboratory for Physical Sciences at Microscale, University of Science and Technology of China, Hefei, Anhui 230026, China. E-mail: jlyang@ustc.edu.cn, jghou@ustc.edu.cn; Fax: +86 551-3602969; Tel: +86 551-3606408

Bin Li

Bin Li received his PhD in physics from University of Science and Technology of China (USTC) in 2002 under the supervision of Prof. Jian Guo Hou. He had then worked as a postdoc in Prof. C. T. Chan's group at the Hong Kong University of Science and Technology, and as a visiting scholar in Prof. W. T. Yang's group at Duke University. From 2005, he is an associate professor at USTC. His research interests include density functional theory, STM simulation, and field emission modeling.

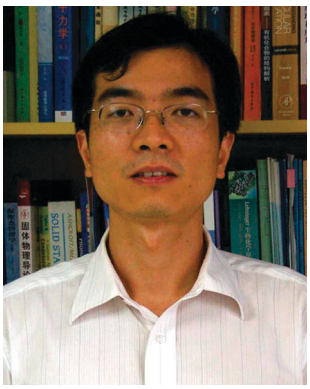

Zhenyu Li

Zhenyu Li received his PhD in chemistry from USTC in 2004 under the supervision of Prof. Jinlong Yang. Since then, he has been working as a post-doctoral researcher in Prof. D. S. Kosov's research group at University of Maryland, College Park and in Prof. Shaul Mukamel's group at University of California, Irvine. Currently, he is an associate professor at USTC. He is the recipient of the national excellent doctoral thesis award. His research interests include electronic structure theory and computation, electron transport in molecular electronics, and theoretical spectroscopy.

laboratory.[14,15] This tool utilizes tunneling current intensity as an observable changing with the coordinate of the detecting tip, and thus achieves the highest spatial resolution until now. Since it was invented, STM has already demonstrated great potentials in characterization and manipulation of various nanostructures, and is becoming a typical and mature technique to explore and control the nano-world.[16–22] The information detected by STM is highly related to the local density of states (LDOS) of the sample near Fermi energy (E_F), as shown by the Tersoff–Hamann approximation,[23,24] which assumes tip states of constant s type of orbital, *i.e.* the idealistic electronic structure, and obtains the tunneling current:

$$I(V_S) \propto \int_{E_F}^{E_F+eV_S} \rho(\vec{r}, E)\mathrm{d}E \quad (1)$$

$$\rho(\vec{r}, E) = \sum_{\mu} |\psi_{\mu}(\vec{r})|^2 \delta(E - E_{\mu}) \quad (2)$$

where $\rho(\vec{r}, E)$ is the LDOS of the sample, E_{μ} is the eigenenergy of the state or molecular orbital $\psi_{\mu}(\vec{r})$ of the sample, and V_S is the sample bias respective to the STM tip. So it is expected that people can observe and manage the molecular orbitals in the STM study of single molecules.

Applications of STM in the study of single molecules began to be popular in the last decade of the 20th century due to rapid developments of the single molecule science. For example, researchers had successfully employed STM to identify adsorption orientations of various molecules on surfaces.[25–27] In recent years, high resolution characterization of single molecules with STM has been further extended to other dimensions, such as chemical bonds resolution[28] and group recognition.[29] Moreover, many of the other physical and chemical phenomena in the STM configuration, such as resonance tunneling,[30,31] single electron tunneling,[32,33] Kondo effect,[19,34] tip-assisted chemical reaction,[22,35] and so on, have been observed and explored. In these studies, the molecular orbitals often act as an important factor assisting in the relevant processes.

The electron tunneling mechanism of STM determines that the obtained information is mainly related to the states (or orbitals) of the sample system near the E_F, *i.e.* the frontier orbitals. For single molecules, energy gaps between the adjacent molecular orbitals are typically quite distinct so that the STM can often map each molecular orbital individually in real space. One may note that STM cannot detect the molecular orbitals far from the E_F due to restriction of the bias voltage in the experiment. However, as suggested by the frontier molecular orbital theory, the molecular orbitals around the E_F determine the reactivity and most of the important properties of the molecular systems. So, exploring the molecular orbitals by high-resolution STM is indeed helpful to enhance our knowledge of the physical, chemical, and other properties of single molecules, and to give a new insight in the potential applications of single molecules in the future industries such as nano-electronics.

In this feature article, we will review and discuss some recent efforts of utilizing STM to characterize molecular adsorption orientation, explore the atomic configuration, analyze the electronic structure, investigate electronic and magnetic behaviors, evaluate interactions between the substrate and molecular sample, and exploit possible applications of single molecules or molecular adsorption systems, in which the molecular orbitals were carefully examined and their vital roles in the related physical/chemical phenomena were revealed.

2. Geometrical characterization

The adsorption configuration of a single molecule on the substrate is one of the fundamental properties that describes an adsorption system. Important geometrical factors include adsorption site, molecular orientation, atomic relaxation of the molecule and surface layer, *etc.* Especially, a single molecule on the substrate usually has a fixed orientation at low temperature, due to the interaction between the molecule and substrate or molecule–molecule interaction. The images scanned by STM reflect the information related to the specific orientation of the molecule, and hence spatial representation of the molecular orbitals. Different orientations may imply different interactions or couplings between the molecule and

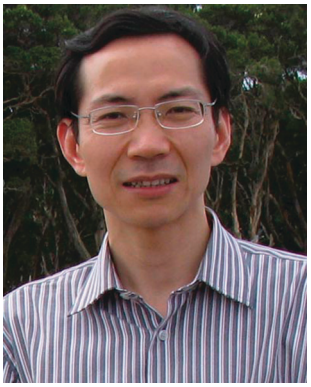

Jinlong Yang

Jinlong Yang, currently a Changjiang professor of chemistry, dean of the School of Chemistry and Material Sciences of USTC, received his PhD in condensed matter physics from USTC in 1991. He is the recipient of the young chemist award from Chinese Chemical Society and the national award (grade two) for natural science, and is the supervisor of two authors of the national excellent doctoral thesis award. His interests focus on developing first principles methods and their application on clusters, nano structures, solid materials, surfaces, and interfaces.

J. G. Hou

J. G. Hou (Jianguo Hou) is a member of the Chinese Academy of Science, president of USTC. He received his PhD in condensed matter physics from USTC in 1989. He is the recipient of the national award (grade two) for natural science, Ho Leung Ho Lee, Qiushi, and Tan Kan Kee awards, and is the supervisor of an author of the national excellent doctoral thesis award. His main research interests focus on characterizing and manipulation at the single molecule scale on surfaces using scanning tunneling spectroscopy.

substrate, resulting in different electronic structures of the frontier orbitals. Therefore, STM observation is essential to firstly identify the molecular configuration on surfaces, and then to explore the physical and chemical properties at the molecule/solid interface.

Adsorption of O_2 molecules on the Pt(111) surface is of concern due to the catalytic action of the Pt surface in oxidation reactions. Two kinds of chemisorbed O_2 molecular precursors are characterized and identified by the high-resolution STM experiment:[36] one is a slightly asymmetric "pear"-shaped pattern in the STM image, ascribed to adsorption at the fcc site of the Pt(111) surface and top-bridge molecular orientation, and another presents a symmetric dimer (or four-leaf-shaped) pattern, corresponding to adsorption at the bridge site and top–top molecular orientation. These two patterns are validated to originate from π^* orbitals of O_2 molecules, and help to determine adsorption sites and orientations of two molecular precursors. For the former adsorption, an appropriate voltage pulse can induce reversible rotation of O_2 molecules among three equivalent orientations at the fcc site, which is revealed by monitoring of the "pear"-shaped pattern.[37]

For larger molecules, the experimental identifications are more complicated and difficult. As a typical three-dimensional molecule, C_{60} has a global shape with all C atoms arranged on its surface, *i.e.* a cage structure. Due to this global shape and atomic homogeneity, C_{60} molecules may present more orientations than small molecules, depending on changes of substrate materials, adsorption site, and other surrounding environments. Then it is an appropriate subject for studying molecular orientations and their effects by the STM technique.

In early STM experiments of C_{60} molecules on metal surfaces, some typical patterns, such as threefold symmetric spots and bright stripes, were often observed. Theoretical simulations based on first-principles had also provided reference to the experimental results. For C_{60} adsorbed on Ag(111) and Au(111) surfaces, a pattern with pentagonal shape at the positive sample bias appeared, obviously resulting from the pentagon structure on the cage of a C_{60} molecule itself, not related to the (111) substrate.[38,39] Hashizume *et al.* found a three-spot pattern of C_{60} adsorbed on the Cu(111) surface with a three-fold symmetry, which may be also related to the distribution of pentagon structures on the C_{60} cage. More importantly, they combined experimental observation and theoretical simulation to identify the orientation of C_{60} molecules,[40] by establishing a relationship between density mapping of the molecular orbitals and the patterns in the STM images. Other efforts were concentrated on the systems of C_{60} adsorbed on semi-conductor substrates, especially the Si surface. Some groups performed the STM experiments of C_{60} adsorbed on Si(111) and Si(100) surfaces, and often observed STM images with a typical pattern of four slightly curved bright stripes.[41–43] It is difficult to directly relate this type of pattern to the geometrical structure of C_{60} molecules. However, a similar pattern was also observed in the case of C_{60} adsorbed on the Au(110) surface,[44] suggesting that the pattern of multiple stripes reflects some information of the structure and specific molecular orbitals of C_{60}.

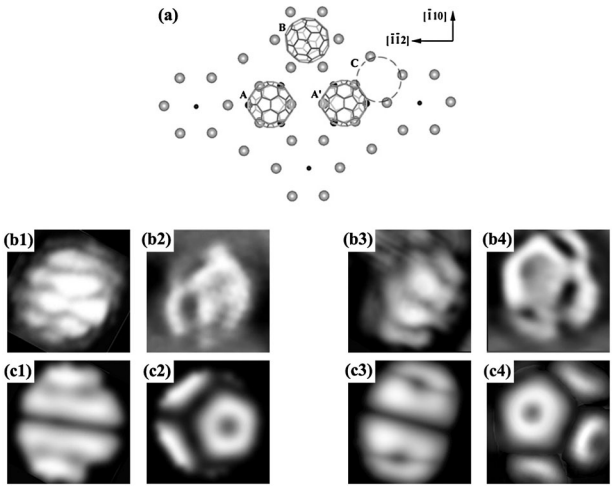

Fig. 1 (a) Schematic of four possible adsorption sites of C_{60} on the Si(111)-(7 × 7) surface: A—faulted half; A′—unfaulted half; B—corner holes; and C—dimer lines. (b) STM images of a single C_{60} molecule with different sample bias voltages V_S: (b1) $V_S = -1.8$ V and (b2) $V_S = 2.5$ V on A sites, and (b3) $V_S = -1.8$ V and (b4) $V_S = 2.3$ V on B sites, with a set-point current I_{set} of 0.15 nA for positive bias images and 0.1 nA for negative bias images. (c) Simulated STM images: (c1) $V_S = -1.8$ V and (c2) $V_S = 2.5$ V with 5–6 bond adsorption on the A site; (c3) $V_S = -1.8$ V and (c4) $V_S = 2.5$ V with edge atom adsorption on the B site. Reprinted figure with permission from ref. 26. Copyright (1999) by the American Physical Society.

All of these patterns were observed and characterized in our low-temperature STM experiment for C_{60} adsorbed on the Si(111)-(7 × 7) surface at ultra-high-vacuum condition.[26] Combining local density approximation (LDA) calculations of C_{60} adsorbed on the Si surface, we can identify the adsorption site and orientation of C_{60} on the Si surface. At higher sample bias with positive polarity, a C_{60} molecule appears as a pentagon adding two or three curved strokes (Fig. 1(b2) and (b4)), which arises from unoccupied molecular orbitals near the E_F of C_{60}, and is identified as specific orientation with both the pentagons and strokes corresponding to the pentagon structures. So we deduced that C_{60} is adsorbed on site A (or A′) of the faulted (or unfaulted) half (see Fig. 1(a)) with one of the 5–6 bonds facing towards the Si surface, while on site B of the corner hole it has one of the edge atoms facing towards the Si substrate (Fig. 1(c)). At other biases, especially the negative sample bias, a type of pattern consisting of a few bright stripes appears (Fig. 1(b1) and (b3)), similar to the experiments by other groups,[41–43] and is from some occupied molecular orbitals of the C_{60} adsorption system. Our study showed that although they can be also used to identify molecular orientation, there exist more complexities from the substrate. The same method was adopted to identify the molecular orientations of C_{60} in a two-dimension molecular lattice[28] and on the surface of a C_{60} island.[45]

Based on the above studies, the pattern at the positive sample bias has become a standard "fingerprint" to determine orientation of C_{60} molecules in many studies.[46–48] It mainly reflects characters of degenerated lowest unoccupied molecular orbitals (LUMO) with t_{1u} symmetry of a C_{60} molecule, because the states derived from the LUMO of C_{60} have fewer

components from the substrate. One can interpret the intra-molecular patterns and then identify the adsorption configurations of single molecules based on the analyses of the molecular orbitals.

In the system of two-dimensional molecular layer, chirality is an important factor because constructing a chiral surface is a crucial step for enantioselective heterogeneous catalysis in chemical and pharmaceutical industries. STM had been employed to characterize various chiral phenomena such as chiral resolution,[25,49] chirality amplification,[50] chiral phase transition,[51] and loss of chirality[52] at the sub-molecular scale in the molecules/substrate systems. In some cases, the chiral character can be related to various orientations of the molecule, so characterizing orientations of chiral molecules is a vital step to explore the chiral nature of the molecular monolayer.

For some molecular systems, the usual STM images can reflect most of the structural characters of the molecule itself, so the chirality of a single molecule can be resolved by directly observing the high-resolution STM images.[25,49,53–55] Lopinski *et al*. have successfully characterized chiralities of alkene molecules on the Si(100) surface.[25] Since the STM images are dominated by individual methyl groups, of which the positions and orientations are related to the chiral character of 2-butene molecules, they can distinguish between *trans*-2-butene and *cis*-2-butene, thus absolute configuration (*R* or *S*) for each of the chiral centres.[25]

Unfortunately, there are still many molecules for which we cannot present an STM image with enough information directly reflecting their atomic configurations. In this situation, theoretical simulation should be helpful to relate some special patterns in an STM image to crucial structural characters of a chiral molecule. When we characterize self-organization of racemic mixtures of 8-nitrospiropyran (SP8) molecules (Fig. 2(a)) on Au(111) by STM, a main difficulty is that the pollywog-like pattern of a single SP8 molecule (Fig. 2(c1) and (c2)) cannot directly show which chirality is possessed by each SP8.[56] So we performed a density functional theoretical (DFT) calculation for an isolated SP8 molecule to interpret the STM images. The calculation indicated that the highest occupied molecular orbital (HOMO) of SP8 is mainly localized around the indoline moiety (Fig. 2(b)). So by comparing the experimental images at the negative sample bias and the calculated spatial distribution of HOMO, we found that every λ-quatrefoil (δ-quatrefoil) contains two face-to-tail coupled SS (RR) dimers and two back-to-back coupled RR (SS) dimers (Fig. 2(d1) and (d2)), and in each dimer two antiparallel homochiral SP8 molecules have the same adsorption orientation on Au(111).[56] It was also deduced that both of the two mirror-imaged 2D chiral structures are not chirally pure but racemic 2D crystals. The adsorption and chiral expression of 6-nitrospiropyran (SP6) molecules on Au(111) were also explored by combining the STM experiments and theoretical calculations.[57] We revealed a unique chiral phenomenon—quasi chiral separation in a 2D orientationally disordered system.

Combination of the high-resolution STM experiments and theoretical calculations has also become a popular method to identify the configuration for other systems, especially the adsorption site and orientation of various molecules, by examining appearances of the molecular orbitals. Bocquet *et al*. used a low-temperature STM to characterize the adsorption of ethene on a well-defined Ag{111}-p(4 × 4) + $Ag_{1.83}O$ reconstructed substrate, in order to study the partial oxidation of ethene on the Ag surface.[58] By comparing the obtained STM images, which have detailed patterns of the molecule and underlying oxide, with the DFT simulated results for various

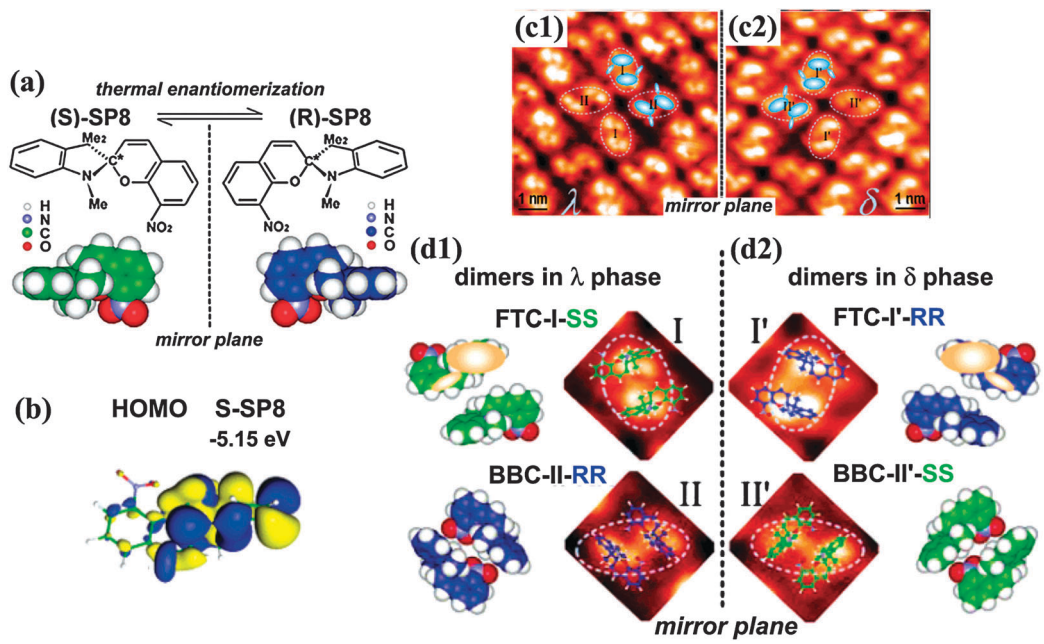

Fig. 2 (a) Molecular structures and models of left-handed (*S*-) and right-handed (*R*-) SP8. (b) Calculated HOMO of a free *S*-SP8 molecule. (c1) and (c2) STM images of λ and δ phases, with $V_S = -0.8$ V and $I_{set} = 0.05$ nA. (d1) and (d2) STM images and proposed models of the four chiral dimers: I, II, I′, and II′. Reprinted with permission from ref. 56. Copyright 2007, American Chemical Society.

possible adsorption configurations, they deduced a convincing orientation and adsorption site of the ethene with respect to the oxide rings.

3. Chemical characterization

Generally, each molecular orbital has its special distribution of the electronic density in space, related to different components of atomic species in it. This implies that the STM image of a single molecule, which only reflects information of the molecular orbitals near the E_F, often cannot be consistent with molecular topography. This complexity of spatial localizations of the molecular orbitals brings lots of difficulties in characterizing a single molecule, but it may be possible to identify some more basic functional components, such as specific atoms, groups, chemical bonds, *etc*. So, we go beyond simple geometrical characterization to chemical characterization.

Still adopting a single C_{60} molecule as a typical example, we tried to present a clearer picture of its cage structure by STM. Although the bright spots in the STM image of C_{60} at the positive sample bias can be related to the pentagons on the cage by examining its LUMO, this corresponding relationship is indirect for observing the cage structure. Due to the molecule–substrate interaction, the STM image at the negative sample bias, *i.e*. the spatial distribution of occupied orbitals of C_{60}, has always irregular patterns compared to that at the positive bias in many cases. In order to reduce this effect, we thermally evaporated a sub-monolayer of C_{60} molecules onto an inert alkanethiol self-assembled monolayers (SAMs) substrate that was prepared on the Au(111) surface and transferred into an STM chamber beforehand.[28] The observed STM image at the negative sample bias, which is contributed by the degenerated HOMO with h_u symmetry of C_{60}, revealed a clear intra-molecule pattern that closely matches the well-known cage structure (Fig. 3(a) and (b)).[28] Especially, the specific distribution of the HOMO of C_{60} results in that its C–C single bonds and C=C double bonds can be markedly distinguished by different contrast of patterns, which means chemical bond resolution.

Identifying atomic species in a single molecule is a pivotal step to realize chemical characterization. Generally, different types of atomic species related to the change of chemical bonding can be often easily distinguished in their STM images. For example, after evaporation of Co onto a monolayer of tetraphenylporphyrin (2HTPP) molecules adsorbed on the Ag(111) surface, the patterns in the center of some molecules changed from depression to protrusion, suggesting a direct metalation of Co atoms with 2HTPP to form Co tetraphenylporphyrin (CoTPP) molecules.[59] This phenomenon can also appear in the cases where different atoms reside in similar chemical bonding environment, such as metal phthalocyanine (MPc) molecules with different central metal ions being 3d transitional elements in the same row (M = Fe, Co, Ni, Cu).[60–62] Both FePc and CoPc molecules presented a pattern of protrusion in their centers, but for NiPc and CuPc a simple dark spot appeared (Fig. 4). Combining the theoretical calculation, researchers deduced that characteristic of d-orbital of the central ion near the E_F is the main origin of different patterns. In FePc and CoPc, the molecular orbitals near the E_F have larger components from d_{z^2} orbitals of the central ions, which is believed to contribute a strong tunneling current, but in the other two molecules this type of orbitals is far from the E_F. STM observation of VOPc molecules was also performed,

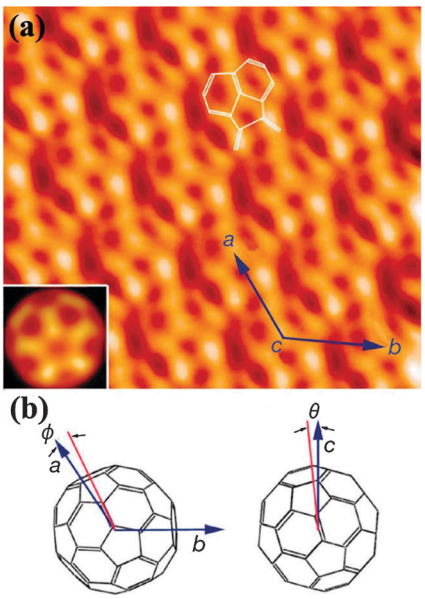

Fig. 3 (a) STM image of a C_{60} lattice measured at 5 K with −2.0 V sample bias. The theoretically simulated STM image is displayed in the inset. (b) Top view (left) and side view (right) of a stick model showing the C_{60} orientations deduced by simulation. The *c*-axis points out of the image. Reproduced with permission from ref. 28. Copyright 2001, Nature Publishing Group.

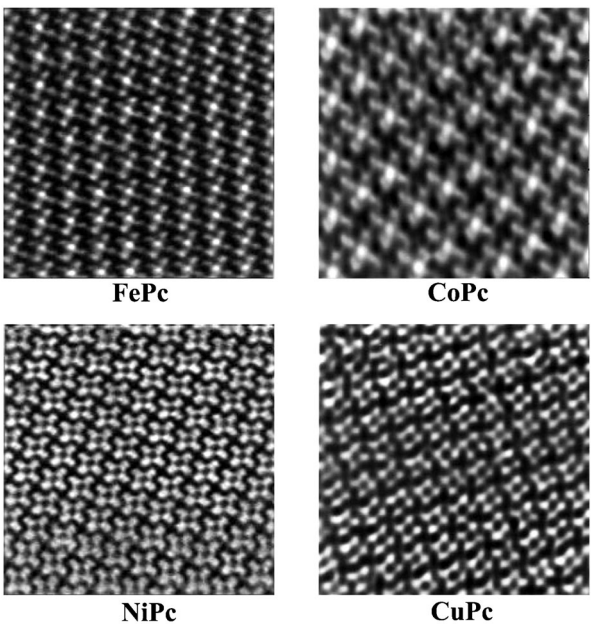

Fig. 4 STM images of four MPc (M = Fe, Co, Ni, Cu) molecules on Au(111) surfaces: a 0.3 nm thick layer of FePc (V_S = 0.10 V, I_{set} = 1.6 nA), a 0.3 nm thick layer of CoPc (V_S = 0.90 V, I_{set} = 0.2 nA), a 0.4 nm thick layer of NiPc (V_S = 0.50 V, I_{set} = 0.3 nA), and a 0.3 nm thick layer of CuPc (V_S = 0.94 V, I_{set} = 0.14 nA). Reprinted with permission from ref. 60 and 62. Copyright 1996 and 1997, American Chemical Society.

and the central pattern appeared to have nodal planes although the O atom is pointed outward the surface, which is attributed to that the molecular orbitals near the E_F have little component around the O atom.[63] The chemical characterizations of the central metal atoms in these macrocyclic compounds have provided main electronic features for their possible usages in many fields.

The characterization of atomic species in a single molecule by STM can be extended to functional groups. The difference between apparent shapes in STM images of CoPc and CoTPP molecules is obvious due to their very different surrounding macrocycles.[64] On the other hand, in the STM study of chloronitrobenzene (ClNB) molecules on the Cu(111) surface, three isomers of ClNB with different positions of substitutional groups were identified, which was thought to result from certain independence of the electronic structure of different parts of the molecule, *i.e.* the special localization of each molecular orbital on different groups.[65] The adsorption configurations of *trans*- and *cis*-2-butene molecules on the Pd(110) surface were explored by comparing localized distributions of their HOMO with the negative bias STM images: the *trans*-2-butene appears as a paired protrusion, with two bright spots corresponding to the positions of CH_3, so a bent adsorption configuration of the C=C–C was identified;[66] an asymmetric head–tail pattern was revealed for the *cis*-2-butene, with the head corresponding to the area where two CH_3 species are located, and an adsorption model of π-bonding at the carbon double-bond on the terminal site of Pd(110) was deduced based on the experiment of rotating the molecule around a single Pd terminal site.[67] Identifying different groups in the same molecule is another essential and challenging step in the chemical characterization. STM observations for 7-alkanethiol SAMs on the Au(111) surface revealed bias-dependent patterns of single molecules: at a positive sample bias up to 1.5 V, all of four 7-alkanethiol molecules in a two-dimensional unit cell of the SAMs show a similar pattern of one spot with different brightness; at a positive sample bias larger than 1.5 V, the patterns of three molecules with lower brightness turn to a stripe; at a negative sample bias, these three molecules appear to be a dimer consisting of two spots.[29] By combining the experimental observations and the first-principles theoretical calculation/simulation, we drew a conclusion that both the elongated part at the higher positive bias and the second spot at the negative bias reflect information about the CH_2 group adjacent to the terminal CH_3 group of the alkanethiol molecule.[29,68] Here the energy-dependence of location of the molecular orbitals at different groups plays an important role in our STM characterization. By changing the sample bias voltage in STM measurement, we can detect different molecular orbitals with different components of each group, so as to resolve and distinguish the terminal CH_3 group and its adjacent CH_2 group.

4. Electronic structure characterization

The bias-dependent STM images of single molecules, such as those in the study of 7-alkanethiol SAMs on Au(111) discussed above, suggested that if the distribution of molecular orbitals can be detected simultaneously in the real and energy spaces, we will obtain more comprehensive information about the electronic states of a single molecule. The STM dI/dV mapping technique just meets this requirement. It integrates energy-resolved tunneling spectroscopy, which was known as scanning tunneling spectroscopy (STS) previously, into a spatial-resolved imaging procedure by STM. Making use of this technique, one can further examine the molecular orbital itself and other information about the electronic states of a single molecule, with the spatial and energy resolutions being realized simultaneously.

The first attempt of this technique occurs in the STM study of C_{60} adsorbed on the Ag(111) surface.[69] In the experiment, dI/dV spectra were measured through lock-in detection of the ac tunneling current. Positioning the STM tip at each point with constant current conditions and then measuring dI/dV signals, one will obtain a series of dI/dV images corresponding to different bias voltages. Since the tunneling current is proportional to the integral of LDOS of the sample in the energy interval restricted by the sample bias according to Tesoff–Hamann approximation[23,24] (also see eqn (1) and (2)), the dI/dV mapping image for a single molecule is thought to directly reflect spatial distribution of each molecular orbital with eigen-energy corresponding to the applied bias voltage. Compared with general STM topography images under the constant current condition, dI/dV mapping images of C_{60} on Ag(111) revealed more details of LDOS distribution of the adsorbed C_{60} with direct orbital resolution.[69] Especially, two dI/dV mapping images from molecular orbitals due to the splitting of LUMO of the adsorbed C_{60} were observed, exhibiting visual influence of the Ag(111) substrate on the electronic structure of C_{60}. These results were validated by theoretical simulations of the dI/dV mapping images.[69,70] The adsorptions of C_{60} molecules on Au(111)[71] and Cu(111)[72] surfaces had also been explored by the dI/dV mapping technique, which presented helpful information to identify the substrate-modified electronic structures and adsorption configuration of single C_{60}.

The dI/dV mapping technique was also employed to study endohedral metallofullerene DyC_{82} molecules,[73] which is one of the fullerene derivatives. Location of metal atoms inside the fullerene cage and metal–cage interaction are always two important issues of the endohedral metallofullerenes, and conventional experimental methods encountered many difficulties in exploring these issues of a single endohedral metallofullerene molecule. STM topography images cannot alone provide enough information to deduce the orientation of DyC_{82} molecules, because of complexities from the low symmetry of this molecule. The dI/dV mapping images at a sample bias around 2.0 V can reveal two molecular orbitals with a pattern of a locally bright ring or dot (Fig. 5(a) and (b)). The related theoretical calculation and simulation validated these two orbitals, which are hybrid states between the fullerene cage and Dy atom (Fig. 5(c) and (d)). The observations of these two molecular orbitals with special patterns related to the Dy atom helped to determine the location of Dy, and also made it possible to identify the orientation of a single DyC_{82} molecule on the Ag/Si surface (Fig. 5(e)).[73]

In some STM investigations of special states related to the systems of single molecules, the dI/dV mapping technique also

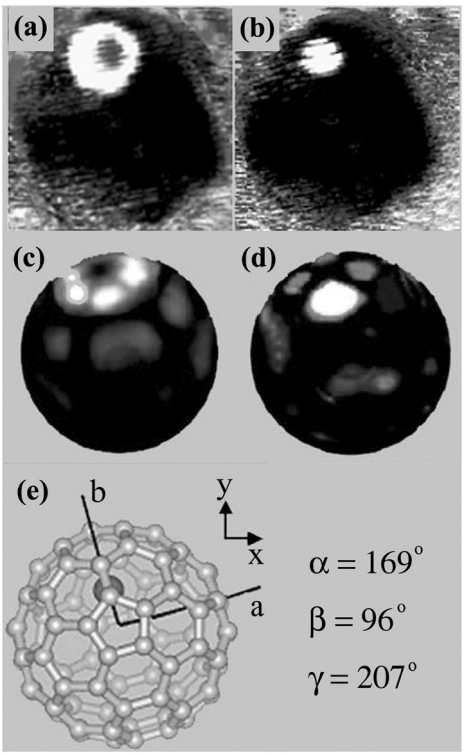

Fig. 5 (a) and (b) dI/dV maps of a Dy@C_{82} molecule with V_S = 2.0 and 2.1 V. (c) and (d) simulated dI/dV maps of a Dy@C_{82} molecule with energies of 1.95 and 2.05 eV relative to the E_F, and (e) molecular orientation on the Ag surface. Three Euler angles are relative to the standard molecular orientation defined in the inset. Reprinted figure with permission from ref. 73. Copyright (2003) by the American Physical Society.

played a pivotal role. Nazin *et al*. used the STM manipulation technique to create a model of molecular junction formed by one CuPc molecule bonded to two Au atomic chains on the NiAl(110) surface.[74] These artificial nanostructures with varying number of Au atoms were characterized by site-dependent dI/dV spectra and dI/dV mapping images, which present abundant information of this structure, such as splitting and shifting of the molecular orbitals after bonding to Au chains, formation of "extended molecule", and modification of the local electronic structure of the Au atomic chains. With the help of the dI/dV mapping technique, Feng *et al*. found a series of atomlike, hollow-core-bound molecular orbitals of C_{60} on the Cu(111) surface at the energy higher than 3.5 eV relative to the E_F (Fig. 6).[75] These special superatom molecular orbitals (SAMO) are induced by the central potential binding of an electron to its screening charge, and were also observed in other nanostructures formed by the C_{60} molecules with hybridization behaviors similar to those of s and p orbitals of H and alkali atoms.

Of course, some of other physical or chemical characteristics related to the electronic structure of single molecules were also experimentally detected by the STM. A typical example is the vibration mode of a single molecule. Inelastic electron tunneling spectroscopy (IETS) had been often measured *via* d^2I/dV^2 signal in STM experiments to characterize the vibration modes of various molecules.[76–79] It was revealed that the symmetry of

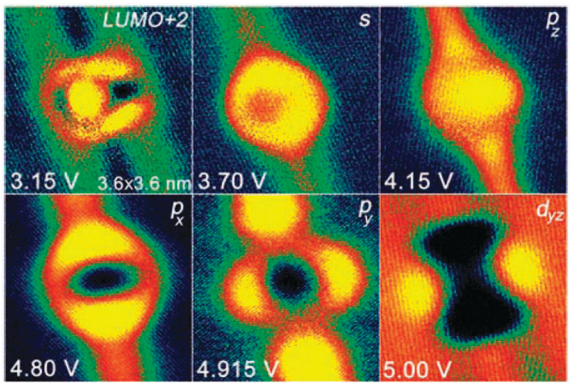

Fig. 6 dI/dV mapping of an individual C_{60} molecule's LUMO + 2 and five SAMOs with core-centered s, p_z, p_x, p_y, and d_{yz} characters, respectively. The sample bias values are labeled at left-down corner. Reproduced with permission from ref. 75. Copyright 2008, American Association for the Advancement of Science.

spatial distribution of vibrational intensities is determined by the symmetry characters of the vibrational mode and the molecular orbitals near the E_F jointly according to a special symmetry selection rule.[76,77] This interesting correlation between the molecular orbital and vibrational mode provides an explicit example of the molecular orbitals being involved in and playing a role in complex physical and chemical processes of single molecules.

5. Spin state characterization

In recent years, functional molecules with specific spin states have received many attentions, due to their potential applications in molecular electronics and spintronics.[80–83]

Investigations of these molecules will improve our knowledge of magnetism and spin-related transports of the molecules at low dimensions. Obviously, it is an essential step in these studies that one can identify the spin state, or magnetic moment at least, of a single molecule. The spin state of a single molecule results from spin-polarized electronic distributions in the molecular orbitals, especially in the frontier orbitals, which often determine main properties of a single molecule acting as a device component in spintronics. So the STM is expected to detect spin states of a single molecule since it has the unique ability of high-resolution characterization for the molecular orbitals near the E_F.

A popular method to detect the spin states of single molecules by using the STM is related to observation and exploration of the Kondo effect. This effect originates from coupling between localized spin and conduction electrons, and can be observed in transport properties through scattering and resonance mechanisms at low temperature.[84] Stimulated by studies of single magnetic atoms, Kondo resonances of molecular complexes formed by a single Co atom or Co dimer bonded to several CO molecules were investigated,[85] and dI/dV mapping at the Kondo resonance was used to locate the source of the spin state of these molecular complexes. Recently, the MPc molecules have been also adopted in the studies of the Kondo effect because of their stable metal–ligand structures.[86] After cutting away eight H atoms from

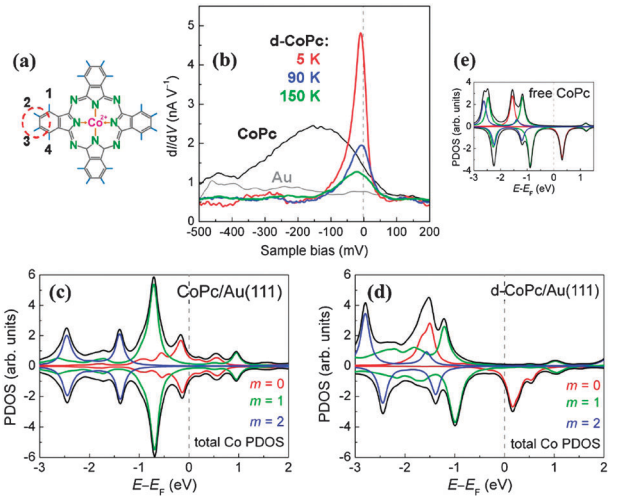

Fig. 7 (a) Structural formula of a CoPc molecule, with H atoms 2 and 3 of one lobe being "cut" by using pulse of STM tip. (b) Typical dI/dV spectra measured at centers of a CoPc molecule with temperature of 5 K (black line), showing a d_{z^2} orbital-mediated tunneling resonance, and a d-CoPc molecule with temperatures of 5, 90, and 150 K (colored lines), showing strong Kondo resonance near the E_F. (c) and (d) PDOS of the Co atom in the CoPc and d-CoPc molecules on the Au(111) surface. (e) PDOS of the Co atom in a free CoPc molecule. Reproduced with permission from ref. 19. Copyright 2005, American Association for the Advancement of Science.

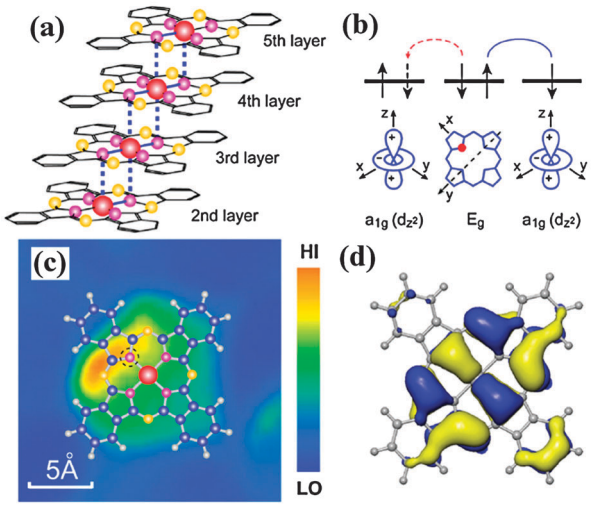

Fig. 8 (a) Illustration of the superexchange interaction and (b) its spin configuration in a molecular chain of CoPc. (c) Spin-flip image of a CoPc molecule on the third layer with temperature of 0.4 K and V_S = −17.2 mV, superimposed upon by the molecular structure. (d) Wavefunction plot of E_g orbital obtained by the first-principles calculation. Reprinted figure with permission from ref. 34. Copyright (2008) by the American Physical Society.

lobes of a CoPc molecule on the Au(111) surface by the STM tip (Fig. 7(a)), one can observe the Kondo resonance which disappears in the case of intact CoPc on the Au(111) surface (Fig. 7(b)).[19] It is attributed to the fact that the lobes of the dehydrogenated CoPc (d-CoPc) molecule are chemically bonded to the Au(111) surface, and then Co–substrate interaction is weakened, resulting in the quenched magnetic moment of the Co ion being restored (Fig. 7(c)). In this study, the change of the spin state of a CoPc molecule, which is directly related to a molecular orbital dominated by the d_{z^2} orbital of the Co ion (Fig. 7(d)), was expressly revealed by examination of the Kondo resonance. Subsequent STM studies showed that the Kondo resonance can be often observed for a single MPc molecule with M being the magnetic metal atom adsorbed on different substrates at appropriate conditions.[87–89] The dI/dV mapping at Kondo resonance energy suggested that the Pc ring besides the central metal ion participates in formations of the spin state and Kondo resonance.[88] Especially, a careful examination, which combined spin-flip IETS at the Kondo resonance of a CoPc molecular film and spin-polarized DFT calculations for the molecular orbitals of CoPc, had helped researchers to identify an E_g molecular orbital belonging to the π system of the phthalocyanine ring of CoPc, which mediates superexchange interaction between the neighboring CoPc molecules and makes two adjacent Co^{2+} ions magnetically linked (Fig. 8).[34] For another molecule TBrPP–Co with a similar metal–ligand structure to the MPc, the spin state of the central Co ion and consequently the Kondo resonance were also characterized and their changes with varied molecular configuration were found.[90] The observations of Kondo resonance and its dI/dV mapping of the TTF–TCNQ complex film on the Au(111) surface showed that the electron acceptor of the film possesses a spin-1/2 ground state due to localization of an unpaired electron in the conjugated LUMO, and the π character of this molecular orbital leads to a split of the Kondo resonance in vibrational sidebands.[91]

The spin detection by using the Kondo resonance has some intrinsical difficulties, such as the fact that the local spin state is not an exclusive precondition of the Kondo resonance. A new thought is to utilize a spin-polarized STM tip, and selective electron tunneling between spin-polarized electronic states (or molecular orbitals) of the sample and tip is expected to guide our identification of the spin state of a single molecule. In the spin-polarized STM experiment of CoPc adsorbed on Co nanoislands grown onto the Cu(111) surface,[92] a Co-coated metal tip, which possesses an out-of-plane component of the magnetization parallel to Co island magnetization, was employed to detect the spin state of the adsorbed CoPc molecule. By comparing the dI/dV spectra and mapping images with obvious spin-polarized electronic resonances on the Co islands and at the central Co ions of CoPc, researchers identified stationary spin states of the adsorbed CoPc molecules, which reflect two molecular spin orientations as a consequence of the ferromagnetic coupling between the molecular spin and the magnetic substrate.[92] With an excellence of sensing stationary spin orientations, this method can play an important role in detecting the spin states of more magnetic molecules and exploring the magnetic interaction between the molecule and environments. But a main difficulty of this method is preparing and characterizing an appropriate spin-polarized STM tip.

6. Molecule–substrate interaction characterization

In common STM experiments of single molecules, the molecules inevitably interact with their surrounding environments

via various ways. Although some STM studies put single molecules onto inert substrates with special purposes of obtaining isolated molecules and their intrinsic natures, most of the STM experiments still choose conducting substrates which generally have non-negligible coupling with the molecules to expand the tunneling channels and thus enhance qualities of the STM images. So the molecule–substrate interactions, in which interplay between the molecular orbitals and substrate states plays a dominated role, are often significant factors in exploring many phenomena and processes at the nano-scale. Types and intensities of the molecule–substrate interactions vary within a broad range, dependent on different species of the molecule and substrate.[93] In cases of weak interactions, there is only a little charge transfer between two sub-systems, with the molecular orbitals being almost unchanged except for their occupations near the E_F. This enables the STM to detect distinct information of the molecular orbitals very close to that of a free molecule. If the interactions are strong enough, large numbers of complex recombinations between the molecular orbitals and substrate states will dominate the electronic structure of the adsorption system, leading to that a lot of molecular orbitals are difficult to be correctly characterized. Of course, most of the situations actually lie between the above two possibilities, so exploring and describing these interactions are complicated and challenging. In detail, the molecular orientations on the substrate, the molecular adsorption site, the bonding configuration, the charged transfer, the matching relationship between the frontier orbitals of the molecule and substrate, and so on, should be examined seriously to obtain a reasonable characterization of effects of the molecule–substrate interactions on the molecular orbitals.

A widely studied system is CO molecules adsorbed on a metal surface. STM observations by Eigler *et al.*[94,95] and the related simulation by Bocquet and Sautet[96] for CO on the Pt(111) surface showed that the molecular patterns mainly originating from the 5σ molecular orbital are dependent on the molecular adsorption site: a high bump at the top site, a low bump surrounded by a circular depression at the bridge site, and a lower bump with a deeper depression at the hollow site. When CO is adsorbed on the Cu(111) surface, it was only observed as a dark depression,[97] which has been recently considered as a result of DOS depletion near the E_F due to strong coupling between the 5σ molecular orbital of CO and $4p_z$ surface state of the Cu surface.[98] Similarly, an anti-bonding state between $1e_{1g}$ molecular orbital (HOMO) of benzene and Pd 4d orbitals was observed in the adsorption system of Pd(110)-c(4 × 2)-benzene.[99]

Although simple situations of the molecular orbitals and bonding mechanisms of small molecules such as CO make them appropriate as prototypes for scientific exploration, the strong molecule–substrate interactions often bring many difficulties in inspecting their molecular orbitals. So here we could examine the C_{60} molecule again because of its good stability and well-characterized HOMO and LUMO at both energy and spatial scales. In the high-resolution STM experiment of C_{60} molecules on the Si(111)-(7 × 7) surface performed at 4.3 K,[26] the STM images at high enough positive biases presented a clear pattern very close to the spatial distribution of LUMO of an individual C_{60} molecule, but it is difficult to directly relate the images at negative biases to the HOMO of an individual C_{60} molecule, because occupied states near the E_F have much components from the Si substrate. Calculations further showed that the C_{60} is bound with the Si substrate by covalent bonds with a small amount of ionic bonds mixed in.[26] This strong interaction modulates the electronic structure of the C_{60} molecule and brings a stripe-like pattern in negative bias images. The selective mixings between different C_{60} molecular orbitals and the substrate states were also traced in cases of the C_{60} adsorbed on other substrates,[38] and may be from specific energy or spatial distribution of substrate bands near the E_F coupling strongly with certain C_{60} molecular orbitals. On the other hand, the site-dependent STS measurements showed that the STS characteristics at different sites are more similar for the unoccupied states than for the occupied states (Fig. 9), which also suggests that the occupied orbitals of C_{60} mix with the Si surface states more than the unoccupied orbitals of C_{60}. Moreover, from the shift of the state derived from LUMO (denoted as LUMO′) toward the E_F in the measured STS, one can determine the order of the charge transfers from the Si surface to C_{60} at different adsorption sites.[100] At the site with the most charge transfer, larger spacing between two adjacent Si atoms makes it possible for sp^3 hybridizations between the carbon and Si atoms[101] to occur on two separated carbon atoms of a C_{60} molecule, which benefits the adjustment of the bonding angle to a lower energy state.

For the C_{60} molecule adsorbed on the Au (111) surface, it was found by combining the STS measurements and dI/dV mapping that only the state LUMO′ has been obviously affected by the adsorption site:[102] the C_{60} molecule adsorbed on the top site has a sharper LUMO′ peak with a little charge transfer from Au to C_{60}, and the C_{60} on the bridge site presents a broader LUMO′ peak with stronger C_{60}–Au interaction. Theoretical simulation based on the DFT calculations revealed that the most stable adsorption orientations of C_{60} molecules are a pentagon facing the surface at the top site and

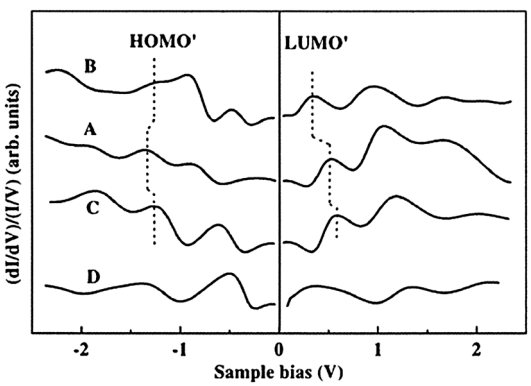

Fig. 9 Curves A, B and C are the averaged STS results corresponding to C_{60} adsorbed at sites A, B, C on the Si(111)-(7 × 7) surface (see Fig. 1), and curve D is the averaged STS on the Si(111)-(7 × 7) surface, respectively. Reprinted figure with permission from ref. 100. Copyright 1999, Elsevier.

a hexagon facing the surface at the bridge site, respectively, with the latter having larger adsorption energy and electron transfer than the former.[103] STS curves simulated by the Gaussian embedded-cluster method (GECM) on the basis of the above configurations presented similar characteristics to the experimental data at two adsorption sites.[103] If the direct coupling between the molecule and Au substrate is further weakened by other ways, such as the electrostatic attraction of electron rich and depleted areas of C_{60} and TPA,[48] the LUMO′ peak will be closer to that of a free C_{60} molecule.

The variation of the molecular orbital with different adsorption locations was also characterized in the system of C_{60} on the Cu(111) surface.[104] Near a step edge, there exist three types of C_{60} molecules: one has a pentagon pattern in its topographic STM image, and other two types located on the upper and lower terrace, respectively, have clover-shaped patterns. The first type can easily be identified as C_{60} with a pentagon facing up. Although the latter two types have similar patterns, obvious difference between peaks corresponding to occupied states in their dI/dV spectra appeared: for the clover-shaped C_{60} adsorbed on the upper terrace, the LUMO + 1 derived peak was measured at ~1.50 V, different from ~1.66 V of the clover-shaped C_{60} adsorbed on the lower terrace and the first type, and a LUMO + 2 derived peak was found in the measurement range. Further dI/dV mapping for LUMO-b and LUMO + 1 derived peaks revealed that the clover-shaped C_{60} adsorbed on the lower terrace is adsorbed with a hexagon parallel to the Cu(111) surface, whereas the one on the upper terrace has a slight departure from the former, with a hexagon not perfectly parallel to the Cu(111) surface.[104] Thus even subtle variation in the adsorption configuration can indeed bring evident changes of interfacial electronic structures and molecular orbitals derived states.

A comparative STM study was performed for the C_{60} molecules on Au(111) and Ag(100) surfaces to explore the possible effect of the substrate on the molecular orbitals.[71] The dI/dV mapping for two systems presented similar patterns.

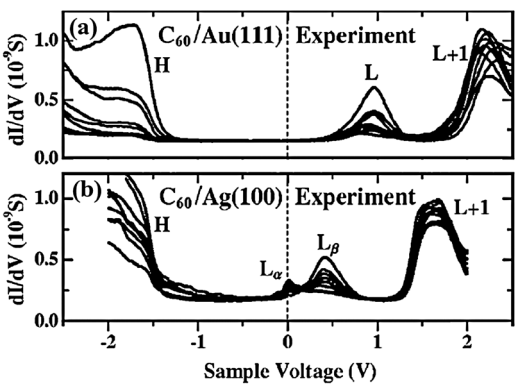

Fig. 10 STS measured at different points on the individual C_{60} molecule on (a) Au(111) and (b) Ag(100) surfaces. H, L and L + 1 denote the HOMO, LUMO, and LUMO + 1 states, respectively. Reprinted figure with permission from ref. 71. Copyright (2004) by the American Physical Society.

Splitting of the LUMO derived peak and decreased HOMO–LUMO gap occur for the C_{60} on the Ag(100) surface with one state pinning at the E_F, in contrast to the suppressed splitting for the C_{60} on Au(111) (Fig. 10). It was attributed to increased screening for the C_{60} on Ag(100) relative to Au(111) due to an increase in the electronic density of states at the E_F for the C_{60} on Ag(100), which is supported by LDA calculation results of more electron transfer for the C_{60} on Ag(100).[71]

In the STM study of the C_{60} monolayer on the Al(111) surface with 6 × 6 periodicity with respect to the substrate mesh, the difference between two kinds of adsorption sites was observed:[105] HOMO and LUMO + 2 of the C_{60} in the STS curve of C_{60} at the 6 × 6 site are shifted further away from the E_F by about 0.2 and 0.35 eV, respectively, compared with those at $2\sqrt{3}$ sites. This was ascribed to variations in molecule–substrate bonding at different adsorption sites. In fact, the 6 × 6 periodicity is formed by raising one-third of the C_{60} molecules (*i.e.* 6 × 6 C_{60}) in the $2\sqrt{3} \times 2\sqrt{3}R30°$ close-packed monolayer as a result of a reconstruction of the underlying Al surface.[106] According to the energy shifts of HOMO and LUMO + 2, one can deduce that the bonding between the 6 × 6 C_{60} and Al(111) substrate is stronger with predominantly covalent character.[105]

The above cases of C_{60} adsorbed on various surfaces illuminate the crucial role of the molecular orbitals in characterizing the molecule–substrate interactions, although some of these studies originally concerned how the interactions influence the molecular orbitals. The frontier molecular orbital theory determines that the energy- and spatial distributions of HOMO, LUMO and other adjacent orbitals of C_{60} are very sensitive to the bonding environment between the molecule and substrate, whereas their appearances in the STM and STS data are still easily identified. So one can choose appropriate molecular orbitals near the E_F to "touch" complicated molecule–substrate interplays in the STM experiment. It is also noted that in the above studies the measured STS data can be considered as evaluation of energy (or bias)-dependent molecular conductivity, which is sensitive to environment of the molecule–substrate interface. Direct relationship between the peak structure in the STS data and the frontier orbitals of the adsorbed molecule deduced from the Tersoff–Hamann approximation[23,24] (see eqn (1)) makes it convenient to study the molecular conductivity and influence of molecule–electrode contact on it at the level of molecular orbitals *via* careful STM examinations.

Most of the above studies are concentrated on the interactions between a single molecule and the perfect substrate. In recent years, scientists have begun to pay attention to defects, dislocation, *etc.* of the imperfect substrate and their derived states, and explore the interactions between the adsorbed molecules and them.[107] In fact, the chemical reactions or processes at the nano-scale often involve special states from the defects of host material. The TiO_2 surface has always attracted many attentions owing to its important applications in heterogeneous catalysis, solar cells, and photocatalysis.[108,109] Bridging oxygen vacancy (O_V), as a type of intrinsic defect, plays a key role in determining electronic and chemical properties of a rutile TiO_2(110)-(1 × 1) surface. The O_Vs constitute not only the most abundant surface donor that

can trap electrons but also act as adsorption sites for simple molecules, so interesting chemistries around the O_V sites have been expected and explored.[110,111] Before studying the interactions and further chemistry between the molecules and the O_Vs on the rutile TiO_2(110)-(1 × 1) surface, we should investigate the frontier orbitals of the O_Vs at the atomic scale. High-resolution STM experiments combined with DFT calculations had been performed to check the O_V defect, and found that occupied orbitals near the E_F resulting from the O_V defect are not localized at the O_V site, but mainly distributed extending over about three neighboring Ti_{5c}^{4+} sites (not including the nearest-neighbor Ti_{5c}^{4+}), with a symmetric four-lobed pattern surrounding the O_V site.[112] This delocalized characteristic of the defect state is ascribed to local lattice distortion and the concomitant change in orbital hybridization,[112] and will obviously influence the adsorption behaviors of small molecules *via* orbital interactions. After CO molecules were evaporated onto the rutile TiO_2(110)-(1 × 1) surface with the intrinsic O_Vs defects at 80 K, STM observation affirmed that at equilibrium the CO molecules are preferentially adsorbed at the next-nearest-neighbor (NNN) Ti_{5c}^{4+} atoms close to the O_Vs and the farther Ti_{5c}^{4+} atoms, with little adsorption probabilities at the O_Vs sites and their nearest-neighbor Ti_{5c}^{4+} atoms.[113] This adsorption preference is consistent with the delocalized distribution of the occupied orbitals resulting from the O_V defect discussed above, and disagrees with an early idea that the O_V itself acts as an adsorption site for the CO molecule.[114,115]

7. Molecular orbitals based engineering

As shown above, STM can characterize abundant structures of single molecules at both energy and spatial spaces. So it has been expected that these properties are helpful to further broaden application prospects of single molecules in the advanced technologies, with the molecular orbitals being the central factor.

Mode-selective chemistry of single molecules adsorbed on a surface has attracted much attention since this new concept is important to controllable chemical reactions at the single molecule scale. In the STM experiment of inducing dissociation of single O_2 molecules on the Ag(110) surface by using electron excitation mechanism, an appropriate voltage pulse at the positive sample bias caused the dissociation of the molecule along [1$\bar{1}$0] direction of the Ag surface, whereas a pulse at the negative sample bias resulted in the dissociation along [001] direction.[116] This dissociation process is related to elongation of the O–O bond due to temporary removal of electrons from the $1\pi_g^{\perp}$ molecular orbital of O_2 or the temporary injection of electrons into this orbital, and before the dissociation along [1$\bar{1}$0] direction a rotation process first happened. Different dissociation pathways under positive and negative voltage polarities were supposed as results of different efficiencies of energy transfer to the rotational mode of O_2 or different barrier to dissociation at two voltage polarities. This experiment revealed the importance of the molecular orbital in the mode-selective chemistry, and also suggested that the reaction pathway may be adjusted by subtle interactions between STM controlling and specific molecular orbital. On the other hand, depending on the spatial distribution of the molecular orbitals near the E_F, the molecular vibrations can be selectively excited by the tunneling electron to realize the mode-selective chemistry of single molecules, as shown by the STM experiment employing inelastic electron tunneling mechanism to induce the S–S bond dissociation of an $(CH_3S)_2$ molecule and the lateral hopping of an isolated CH_3S molecule on the Cu(111) surface.[117] The LUMO of $(CH_3S)_2$ molecule is localized at both the S–S and C–H bonds, so a resonantly captured electron may influence these two bonds. But for the CH_3S molecule, there is no contribution of the molecular orbitals near the E_F to the C–H bond, and the LUMO and LUMO + 1 are rather localized at the C–S bond. These results are consistent with the action spectrum[118] results obtained in the STM experiment.[117] Then the important effects of the spatial distributions and populations of the molecular orbitals near the E_F on the selectively excited vibrational modes and controllable single-molecule chemical reactions are highlighted. Recently, an STM study combined the above two mechanisms to realize the controllable dissociation of a single H_2O molecule adsorbed on the Mg(100) film prepared on the Ag(100) substrate:[119] a lower voltage pulse corresponding to an asymmetric O–H stretching mode (inelastic electron tunneling mechanism) makes the H_2O molecule dissociate into hydroxyl, and a higher voltage pulse corresponding to LUMO energy of the adsorbed H_2O (electron excitation mechanism) obtains the product of atomic oxygen. The crucial functions and potential applications of the molecular orbitals in the mode-selective chemistry are still under exploration and development.

The molecular orbitals of single molecules can also play a key role in designs of nano- and molecular devices. An important example is the $C_{59}N$-based single electron tunneling (SET) device:[33] an individual $C_{59}N$ molecule is put into double-barrier tunneling junctions (DBTJs) constructed in the STM configuration, and interplay between half-occupied HOMO and SET effect is utilized to realize rectifying function. But more molecular devices are based on the coupling between the special electronic structures (or molecular orbital configurations) of the sample molecule and STM electrodes, *i.e.* the STM tip or substrate. In fact, wavefunction coupling between the detected molecular orbitals and the states of the STM tip, which is originally a precondition of STM imaging the sample, and other phenomena such as tip-induced changes of the molecules have made the tip effects dominant in some cases of exploring single molecules.

The STM tip is our "finger" to "touch" single molecules in the STM experiment, so its status is vital to the quality of STM characterizing the molecular orbitals. Before the STM experiment, the tip should be subject to careful cleaning treatment, and theoretically, the frontier orbitals of a "satisfying" STM tip are supposed to be similar to the s-type orbital,[23] or at least have some dominant $m = 0$ contributions near the E_F.[120] But in some cases, we may require a specific STM tip, which has some artificially designed electronic states with selective coupling to the orbitals of the sample molecule, in order to realize specific function that cannot be implemented by a conventionally "satisfying" tip. This selective coupling often makes use of the particular distribution of the molecular

orbitals at the energy and spatial scales, and can be understood *via* the modified Bardeen approximation (MBA):[121]

$$I(V_S) = \frac{4\pi e}{\hbar}\sum_{\mu,\nu}[f(E_\mu) - f(E_\nu)]|M_{\mu\nu}|^2\delta(E_\mu - E_\nu - eV_S) \quad (3)$$

$$M_{\mu\nu} = -\frac{\hbar^2}{2m}\int_\Sigma (\chi_\nu^*\nabla\psi_\mu - \psi_\mu\nabla\chi_\nu^*)d\vec{S} \quad (4)$$

where E_ν is the eigenenergy of the state or molecular orbital χ_ν of the tip, ψ_μ and E_μ have appeared in eqn (1) and (2), $M_{\mu\nu}$ is the matrix element for transition of an electron from ψ_μ to χ_ν, and the Fermi function $f(E)$ is used to choose possible active tunneling orbitals of the sample and tip.

Most of the attempts utilized a chemically modified tip, which is obtained by making some small molecules adsorbed onto the conventional STM tip. Then this chemically modified tip possesses specific electronic states derived from the orbital of those small molecules, and the coupling relationships of the resonant tunneling between these states and the orbitals of the sample molecule will be very explicit. A typical example is the CO-adsorbed STM tip, which was constructed to differentiate between the CO molecule and O atom co-adsorbed on the Cu(111) surface:[97] when using a conventional W tip, they present similar patterns of depression; but when using the CO-adsorbed STM tip, the CO becomes a protrusion, and the O remains unchanged. Combined with the theoretical simulation[122] using the MBA,[121] one can find that enhanced electron tunneling between similar CO $\pi^*_{p_x,p_y}$ orbital-derived states of the sample and tip, because of the same spatial symmetries of their wavefunctions, makes the tunneling current reach its maximum when the CO-adsorbed tip is positioned on the CO molecule on Cu(111). This type of STM tip with a CO molecule as the terminal group was also adopted by Ho's group to identify the adsorption sites and orientations of some molecules/atoms on the substrate.[35,76,123] For example, O_2 molecules adsorbed on the Ag(110) surface reflected itself as a depression, but if the CO-adsorbed tip is used, the pattern turns into a bright dimer, which was thought to correspond to adsorption appearance of the O_2 molecule.[76] Theoretical simulation[122] verified this assumption: the electron tunneling between the states of the CO-adsorbed tip and adsorbed O on Ag(110) with a similar O $2p_x$ orbital characteristic is enhanced when the tip is positioned upon the O atom.

Another example is the C_{60}-adsorbed STM tip. The frontier of this tip is mainly derived from the HOMO and LUMO of C_{60}, which have more complicated spatial distribution than those of the CO-adsorbed tip, but the discrete characteristic of C_{60} HOMO and LUMO at the energy scale can make this tip suitable to construct some functional molecular devices. The C_{60}-adsorbed STM tip was validated by measuring the HOPG surface[124] and the alkanethiol SAMs surface (Fig. 11(a)).[30] When this tip was positioned upon another C_{60} molecule physically adsorbed on alkanethiol SAMs prepared on the Au(111) surface, a negative differential resistance (NDR) phenomenon occurred in the positive sample bias region of the STS curve (Fig. 11(b)).[30] Here the resonant tunneling

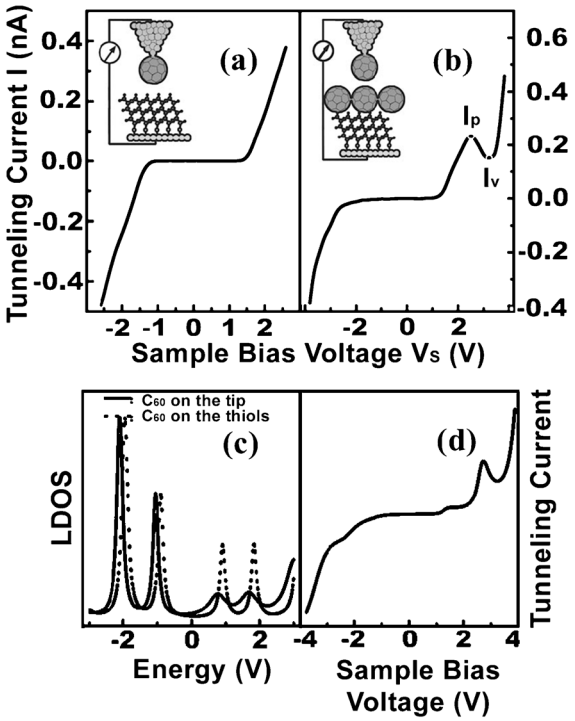

Fig. 11 (a) and (b) *I–V* curves obtained by using a C_{60} tip over the alkanethiol SAMs and the C_{60} films, respectively. (c) LDOS of the C_{60} molecule on the tip and on the alkanethiol SAMs, with different Lorentzian widths being assumed for the occupied and unoccupied states of the C_{60} on the tip, and (d) the corresponding simulated *I–V* curves. Reprinted with permission from ref. 30. Copyright 2000, American Institute of Physics.

between the LUMO of C_{60} on SAMs and the HOMO of C_{60} on the tip is responsible for it, and larger energy gaps between the HOMO (LUMO) and other molecular orbitals promote the formation of this NDR effect. Absence of the NDR in the negative bias region was ascribed to the following fact: for the Pt–Ir STM tip adsorbed with a C_{60} molecule, unoccupied states near the E_F are mainly from C_{60} molecular orbitals mixing with the extended s orbitals of Pt, and they are more extended than occupied states near the E_F that are derived from C_{60} orbitals mixing mainly with the localized d orbitals of Pt (see Fig. 11(c) and (d)).[125]

Except for the chemically modified tip adsorbed with small molecules, the STM tips using other metal materials apart from conventional W and Pt–Ir alloy have been also fabricated and used in STM experiments for specific systems.[126,127] Elaborately designed couplings between some metal tips and the orbitals of sample molecules were displayed in the cases of Ni or Fe tips used to explore CoPc molecules adsorbed on the Au(111) surface.[128,129] As a coordination compound, CoPc has many molecular orbitals with multiform spatial distributions and symmetries around the central metal ion and surrounding ligands, which are kept on the whole even after it is adsorbed onto the Au(111) surface. Adopting a Ni(111) tip in the STS experiment of CoPc/Au(111), Chen *et al.* observed an explicit and stable NDR phenomenon at the negative sample bias when the Ni tip is upon the central Co ion, but the NDR phenomenon did not occur when a W tip was used

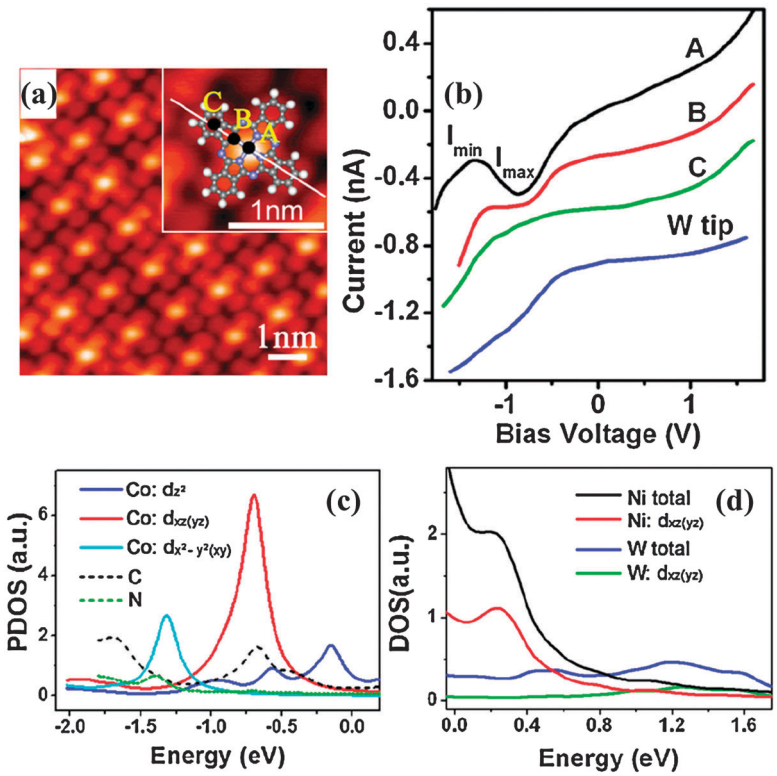

Fig. 12 (a) CoPc monolayer on Au(111) surface (V_S = 1.2 V, I_{set} = 0.2 nA). Inset: a magnified molecule image with a superimposed CoPc ball-stick sketch. (b) *I–V* curves measured with the Ni tip over sites A, B, and C (see the inset of (a)), and with the W tip over site A. The curves are shifted vertically for clarity by separations of 0.3 nA. (c) Calculated PDOS of d orbitals of the Co atom and of C, N atoms in a CoPc molecule adsorbed on the Au(111) surface. (d) Calculated DOS of the Ni and the W tips as well as their $d_{xz(yz)}$ fractions. Reprinted figure with permission from ref. 128. Copyright (2007) by the American Physical Society.

(Fig. 12(a) and (b)).[128] A slight increase of tip offset from the Co atom can make the NDR phenomenon disappear rapidly. So it can be deduced that this NDR effect should be related to a specific coupling relationship, which is spatially local, between one state of the Ni tip and some molecular orbitals of CoPc. Further theoretical calculations and simulation based on the MBA[121] showed that the resonant tunneling modes between an occupied molecular orbital with $d_{xz(yz)}$ characteristic around the Co ion at ~ -0.69 eV relative to the E_F of the adsorbed CoPc (Fig. 12(c)) and some $d_{xz(yz)}$ states at ~ 0.23 eV relative to the E_F of the Ni(111) tip (Fig. 12(d)) result in this NDR effect. On the other hand, in the STS experiment of CoPc/Au(111) a Fe-coated W tip had also been validated to possess an interesting function that cannot be realized by the conventional W tip: it can be used to identify delocalized molecule–substrate hybrid states.[129] These states are derived from the molecular orbitals mainly distributed around the ligands, and are mixed with many components from the Au substrate, so that the W tip with s-like frontier orbitals cannot distinguish them from other states with more molecular components. But the frontier orbitals of the Fe-coated W tip possess extended spatial distribution, so their strong spatial couplings to these hybrid states result in that this tip can detect them in the STS data. An argument was highlighted in these two cases: the molecular orbital, regardless of whether it dominates its derived states in the adsorption system, or it is strongly mixed with the substrate states, can couple with a specially designed STM tip by the spatial resonance and local symmetry matching of the electronic states, to bring new mechanisms and functions of the STM.

The tunneling couplings between the orbitals of the sample molecule and special states of the substrate were also explored and utilized to realize specific functions. The NDR effect was observed in STS of styrene or 2,2,6,6-tetramethyl-1-piperidinyloxy molecules adsorbed on the doped Si(100) surface, with different bias polarities at which the NDR occurs corresponding to different doped types (n- or p-) of the Si substrate.[130] The theoretical analyses showed that this NDR phenomenon is from the resonant tunnelings between the local HOMO or LUMO at the energy scale of the adsorbed molecule and "local states" of the Si(100) substrate. These "local states" are defined in the tunneling mechanism and formed due to doping.[131,132] Compared with the studies of couplings between the orbitals of the sample and tip, this type of exploration has more difficulties, such as that fewer surfaces can be used as the substrate of single molecules in the STM experiment, and that balance between the molecule–substrate interaction and the tunneling coupling is very subtle.

8. Conclusions

With a strong detecting ability deep into the sub-atomic resolution, STM is a powerful technique to investigate properties of single molecules at both spatial and energy scales and to

explore their applications in the future nano-based industries. The imaging mechanism of STM determines that the molecular orbitals of single molecules play a vital role in the STM study of single molecule science. The spatial relationships, such as symmetry and extension, between the atomic structure and molecular orbitals make it possible to study the atomic structure, adsorption site, and relative orientation of single molecules using STM. The specific distributions of the molecular orbitals around different atoms and groups in single molecules are employed to identify the atomic species, chemical bonds and atomic groups, with distinct intra-molecular patterns being assigned accurately in some cases. The dI/dV mapping technique can describe the spatial characteristics of an individual molecular orbital in single molecules, so that it has been used to reveal intrinsic structural and orientational properties of single molecule systems, and to explore unique electronic information of nano-systems related to the molecular orbitals. The spin-related electronic properties of the single molecule system, especially local magnetic moment determined by specific molecular orbitals, were also detected by the STM technique, with the help of characterising the Kondo resonance or selective electronic tunneling between the spin-polarized states of the tip and sample. The substrates have alterable interactions with single molecules, depending on the types of the substrates, and these interactions can be described by checking molecular orbitals on the basis of the STM images and STS measurement. Based on the subtle STM controlling of the molecular orbitals, the mode-selective chemistry can be realized by the electron excitation mechanism and inelastic electron tunneling mechanism. The applications of non-conventional STM tips in the single molecule study are based on the resonance tunneling between the molecular orbitals of the tip and sample at energy and/or spatial scales, which can provide additional information about the single molecule, or present new ideas for designing the nano- and molecular devices. In the above study, the theoretical calculations based on the first-principles and the simulations of STM data, in which the molecular orbitals were important objects under the investigations, were often combined with the STM experiments to explore the nature of single molecules. The molecular orbitals based method successfully applied in the STM studies on single molecules is expected to be further developed and extended to explore many of other fields in the nano-sciences.

Acknowledgements

This work was partially supported by the National Natural Science Foundation of China (50721091, 10874164, 20873129, 10704069, 90921013 and 20933006), National Key Basic Research Program (2006CB922000), the USTC-HP HPC Project, and the SCCAS and Shanghai Supercomputer Centers. We also thank Dr Jin Zhao for her valuable discussions and help.

Notes and references

1 T. H. Lee, J. I. Gonzalez, J. Zheng and R. M. Dickson, *Acc. Chem. Res.*, 2005, **38**, 534.
2 H. Haick and D. Cahen, *Acc. Chem. Res.*, 2008, **41**, 359.
3 B. L. Feringa, R. A. van Delden, N. Koumura and E. M. Geertsema, *Chem. Rev.*, 2000, **100**, 1789.
4 A. de Meijere and H. Hopf, *Chem. Rev.*, 2006, **106**, 4785.
5 R. Klajn, J. F. Stoddart and B. A. Grzybowski, *Chem. Soc. Rev.*, 2010, **39**, 2203.
6 L. F. Lindoy, *Nature*, 1993, **364**, 17.
7 Z. M. Liu, A. A. Yasseri, J. S. Lindsey and D. F. Bocian, *Science*, 2003, **302**, 1543.
8 Y. Zheng, J. J. Neville and C. E. Brion, *Science*, 1995, **270**, 786.
9 H. Song, Y. Kim, Y. H. Jang, H. Jeong, M. A. Reed and T. Lee, *Nature*, 2009, **462**, 1039.
10 L. Scudiero, D. E. Barlow, U. Mazur and K. W. Hipps, *J. Am. Chem. Soc.*, 2001, **123**, 4073.
11 S. Lenfant, C. Krzeminski, C. Delerue, G. Allan and D. Vuillaume, *Nano Lett.*, 2003, **3**, 741.
12 O. V. Pupysheva, A. A. Farajian and B. I. Yakobson, *Nano Lett.*, 2008, **8**, 767.
13 T. Kambe, K. Kajiyoshi, M. Fujiwara and K. Oshima, *Phys. Rev. Lett.*, 2007, **99**, 177205.
14 G. Binnig and H. Rohrer, *Helv. Phys. Acta*, 1982, **55**, 726.
15 G. Binnig, H. Rohrer, Ch. Gerber and E. Weibel, *Phys. Rev. Lett.*, 1982, **49**, 57.
16 T. W. Odom, J.-L. Huang, P. Kim and C. M. Lieber, *Nature*, 1998, **391**, 62.
17 H. C. Manoharan, C. P. Lutz and D. M. Eigler, *Nature*, 2000, **403**, 512.
18 P. A. Sloan and R. E. Palmer, *Nature*, 2005, **434**, 367.
19 A. D. Zhao, Q. X. Li, L. Chen, H. J. Xiang, W. H. Wang, S. Pan, B. Wang, X. D. Xiao, J. L. Yang, J. G. Hou and Q. S. Zhu, *Science*, 2005, **309**, 1542.
20 G. M. Rutter, J. N. Crain, N. P. Guisinger, T. Li, P. N. First and J. A. Stroscio, *Science*, 2007, **317**, 219.
21 J. K. Gimzewski, *Phys. World*, 1998, **11**, 29.
22 S.-W. Hla, L. Bartels, G. Meyer and K.-H. Rieder, *Phys. Rev. Lett.*, 2000, **85**, 2777.
23 J. Tersoff and D. R. Hamann, *Phys. Rev. Lett.*, 1983, **50**, 1998.
24 J. Tersoff and D. R. Hamann, *Phys. Rev. B*, 1985, **31**, 805.
25 G. P. Lopinski, D. J. Moffatt, D. D. M. Wayner and R. A. Wolkow, *Nature*, 1998, **392**, 909.
26 J. G. Hou, J. L. Yang, H. Q. Wang, Q. X. Li, C. G. Zeng, H. Lin, B. Wang, D. M. Chen and Q. S. Zhu, *Phys. Rev. Lett.*, 1999, **83**, 3001.
27 X. H. Qiu, C. Wang, Q. D. Zeng, B. Xu, S. X. Yin, H. N. Wang, S. D. Xu and C. L. Bai, *J. Am. Chem. Soc.*, 2000, **122**, 5550.
28 J. G. Hou, J. L. Yang, H. Q. Wang, Q. X. Li, C. G. Zeng, L. F. Yuan, B. Wang, D. M. Chen and Q. S. Zhu, *Nature*, 2001, **409**, 304.
29 C. G. Zeng, B. Li, B. Wang, H. Q. Wang, K. D. Wang, J. L. Yang, J. G. Hou and Q. S. Zhu, *J. Chem. Phys.*, 2002, **117**, 851.
30 C. G. Zeng, H. Q. Wang, B. Wang, J. L. Yang and J. G. Hou, *Appl. Phys. Lett.*, 2000, **77**, 3595.
31 X. W. Tu, G. Mikaelian and W. Ho, *Phys. Rev. Lett.*, 2008, **100**, 126807.
32 J. G. Hou, B. Wang, J. L. Yang, X. R. Wang, H. Q. Wang, Q. S. Zhu and X. D. Xiao, *Phys. Rev. Lett.*, 2001, **86**, 5321.
33 J. Zhao, C. G. Zeng, X. Cheng, K. D. Wang, G. W. Wang, J. L. Yang, J. G. Hou and Q. S. Zhu, *Phys. Rev. Lett.*, 2005, **95**, 045502.
34 X. Chen, Y.-S. Fu, S.-H. Ji, T. Zhang, P. Cheng, X.-C. Ma, X.-L. Zou, W.-H. Duan, J.-F. Jia and Q.-K. Xue, *Phys. Rev. Lett.*, 2008, **101**, 197208.
35 H. J. Lee and W. Ho, *Science*, 1999, **286**, 1719.
36 B. C. Stipe, M. A. Rezaei, W. Ho, S. Gao, M. Persson and B. I. Lundqvist, *Phys. Rev. Lett.*, 1997, **78**, 4410.
37 B. C. Stipe, M. A. Rezaei and W. Ho, *Science*, 1998, **279**, 1907.
38 E. I. Altman and R. J. Colton, *Phys. Rev. B: Condens. Matter*, 1993, **48**, 18244.
39 E. I. Altman and R. J. Colton, *Surf. Sci.*, 1993, **295**, 13.
40 T. Hashizume, K. Motai, X. D. Wang, H. Shinohara, Y. Maruyama, K. Ohno, Y. Nishina, H. W. Piclering, Y. Kuk and T. Sakurai, *Phys. Rev. Lett.*, 1993, **71**, 2959.
41 T. Hashizume, X. D. Wang, Y. Nishina, H. Shinohara, Y. Saito, Y. Kuk and T. Sakurai, *Jpn. J. Appl. Phys.*, 1992, **31**, L880.

42 X. D. Wang, T. Hashizume, H. Shinohara, Y. Sato, Y. Nishina and T. Sakurai, *Jpn. J. Appl. Phys.*, 1992, **31**, L983.
43 P. Moriarty, Y.-R. Ma, M. D. Upward and P. H. Beton, *Surf. Sci.*, 1998, **407**, 27.
44 R. Gaisch, R. Berndt, J. K. Gimzewski, B. Reihl, R. R. Schlittler, W. D. Schneider and M. Tschudy, *J. Vac. Sci. Technol., B*, 1994, **12**, 2153.
45 H. Q. Wang, C. G. Zeng, B. Wang, J. G. Hou, Q. X. Li and J. L. Yang, *Phys. Rev. B: Condens. Matter*, 2001, **63**, 085417.
46 J. I. Pascual, J. Gómez-Herrero, D. Sánchez-Portal and H.-P. Rust, *J. Chem. Phys.*, 2002, **117**, 9531.
47 G. Schull and R. Berndt, *Phys. Rev. Lett.*, 2007, **99**, 226105.
48 K. J. Franke, G. Schulze, N. Henningsen, I. Fernández-Torrente, J. I. Pascual, S. Zarwell, K. Rück-Braun, M. Cobian and N. Lorente, *Phys. Rev. Lett.*, 2008, **100**, 036807.
49 F. Vidal, E. Delvigne, S. Stepanow, N. Lin, J. V. Barth and K. Kern, *J. Am. Chem. Soc.*, 2005, **127**, 10101.
50 R. Fasel, M. Parschau and K.-H. Ernst, *Nature*, 2006, **439**, 449.
51 S. Weigelt, C. Busse, L. Petersen, E. Rauls, B. Hammer, K. Gothelf, F. Besenbacher and T. Linderoth, *Nat. Mater.*, 2006, **5**, 112.
52 J. Zhang, A. Gesquière, M. Sieffert, M. Klapper, K. Müllen, F. C. De Schryver and S. De Feyter, *Nano Lett.*, 2005, **5**, 1395.
53 P. Messina, A. Dmitriev, N. Lin, H. Spillmann, M. Abel, J. V. Barth and K. Kern, *J. Am. Chem. Soc.*, 2002, **124**, 14000.
54 A. Dmitriev, H. Spillmann, M. Lingenfelder, N. Lin, J. V. Barth and K. Kern, *Langmuir*, 2004, **20**, 4799.
55 J. Zhang, B. Li, X. F. Cui, B. Wang, J. L. Yang and J. G. Hou, *J. Am. Chem. Soc.*, 2009, **131**, 5885.
56 T. Huang, Z. P. Hu, B. Wang, L. Chen, A. D. Zhao, H. Q. Wang and J. G. Hou, *J. Phys. Chem. B*, 2007, **111**, 6973.
57 T. Huang, Z. P. Hu, A. D. Zhao, H. Q. Wang, B. Wang, J. L. Yang and J. G. Hou, *J. Am. Chem. Soc.*, 2007, **129**, 3857.
58 M.-L. Bocquet, P. Sautet, J. Cerda, Ch. I. Carlisle, M. J. Webb and D. A. King, *J. Am. Chem. Soc.*, 2003, **125**, 3119.
59 T. E. Shubina, H. Marbach, K. Flechtner, A. Kretschmann, N. Jux, F. Buchner, H.-P. Steinrück, T. Clark and J. M. Gottfried, *J. Am. Chem. Soc.*, 2007, **129**, 9476.
60 X. Lu, K. W. Hipps, X. D. Wang and U. Mazur, *J. Am. Chem. Soc.*, 1996, **118**, 7197.
61 K. W. Hipps, X. Lu, X. D. Wang and U. Mazur, *J. Phys. Chem.*, 1996, **100**, 11207.
62 X. Lu and K. W. Hipps, *J. Phys. Chem. B*, 1997, **101**, 5391.
63 D. E. Barlow and K. W. Hipps, *J. Phys. Chem. B*, 2000, **104**, 5993.
64 D. E. Barlow, L. Scudiero and K. W. Hipps, *Langmuir*, 2004, **20**, 4413.
65 E. Niemi, V. Simic-Milosevic, K. Morgenstern, A. Korventausta, S. Paavilainen and J. Nieminen, *J. Chem. Phys.*, 2006, **125**, 184708.
66 Y. Kim, T. Komeda and M. Kawai, *Phys. Rev. Lett.*, 2002, **89**, 126104.
67 Y. Sainoo, Y. Kim, T. Komeda, M. Kawai and H. Shigekawa, *Surf. Sci.*, 2003, **536**, L403.
68 B. Li, C. G. Zeng, Q. X. Li, B. Wang, L. F. Yuan, H. Q. Wang, J. L. Yang, J. G. Hou and Q. S. Zhu, *J. Phys. Chem. B*, 2003, **107**, 972.
69 X. Lu, M. Grobis, K. H. Khoo, S. G. Louie and M. F. Crommie, *Phys. Rev. Lett.*, 2003, **90**, 096802.
70 M. De Menech, U. Saalmann and M. E. Garcia, *Phys. Rev. B: Condens. Matter Mater. Phys.*, 2006, **73**, 155407.
71 X. Lu, M. Grobis, K. H. Khoo, S. G. Louie and M. F. Crommie, *Phys. Rev. B: Condens. Matter Mater. Phys.*, 2004, **70**, 115418.
72 J. A. Larsson, S. D. Elliott, J. C. Greer, J. Repp, G. Meyer and R. Allenspach, *Phys. Rev. B: Condens. Matter Mater. Phys.*, 2008, **77**, 115434.
73 K. D. Wang, J. Zhao, S. F. Yang, L. Chen, Q. X. Li, B. Wang, S. H. Yang, J. L. Yang, J. G. Hou and Q. S. Zhu, *Phys. Rev. Lett.*, 2003, **91**, 185504.
74 G. V. Nazin, X. H. Qiu and W. Ho, *Science*, 2003, **302**, 77.
75 M. Feng, J. Zhao and H. Petek, *Science*, 2008, **320**, 359.
76 J. R. Hahn, H. J. Lee and W. Ho, *Phys. Rev. Lett.*, 2000, **85**, 1914.
77 N. Lorente, M. Persson, L. J. Lauhon and W. Ho, *Phys. Rev. Lett.*, 2001, **86**, 2593.
78 J. I. Pascual, J. Gómez-Herrero, D. Sánchez-Portal and H.-P. Rust, *J. Chem. Phys.*, 2002, **117**, 9531.
79 M. Grobis, K. H. Khoo, R. Yamachika, X. Lu, K. Nagaoka, S. G. Louie, M. F. Crommie, H. Kato and H. Shinohara, *Phys. Rev. Lett.*, 2005, **94**, 136802.
80 H. O. Stumpf, L. Ouahab, Y. Pei, D. Grandjean and O. Kahn, *Science*, 1993, **261**, 447.
81 S. Bertaina, S. Gambarelli, T. Mitra, B. Tsukerblat, A. Muller and B. Barbara, *Nature*, 2008, **453**, 203.
82 L. Vitali, S. Fabris, A. M. Conte, S. Brink, M. Ruben, S. Baroni and K. Kern, *Nano Lett.*, 2008, **8**, 3364.
83 H. B. Heersche, Z. de Groot, J. A. Folk, H. S. J. van der Zant, C. Romeike, M. R. Wegewijs, L. Zobbi, D. Barreca, E. Tondello and A. Cornia, *Phys. Rev. Lett.*, 2006, **96**, 206801.
84 A. C. Hewson, *The Kondo Problem to Heavy Fermions*, Cambridge University Press, Cambridge, 1993.
85 P. Wahl, L. Diekhöner, G. Wittich, L. Vitali, M. A. Schneider and K. Kern, *Phys. Rev. Lett.*, 2005, **95**, 166601.
86 Z. Y. Li, B. Li, J. L. Yang and J. G. Hou, *Acc. Chem. Res.*, 2010, **43**, 954.
87 L. Gao, W. Ji, Y. B. Hu, Z. H. Cheng, Z. T. Deng, Q. Liu, N. Jiang, X. Lin, W. Guo, S. X. Du, W. A. Hofer, X. C. Xie and H.-J. Gao, *Phys. Rev. Lett.*, 2007, **99**, 106402.
88 Y.-S. Fu, S.-H. Ji, X. Chen, X.-C. Ma, R. Wu, C.-C. Wang, W.-H. Duan, X.-H. Qiu, B. Sun, P. Zhang, J.-F. Jia and Q.-K. Xue, *Phys. Rev. Lett.*, 2007, **99**, 256601.
89 A. D. Zhao, Z. P. Hu, B. Wang, X. D. Xiao, J. L. Yang and J. G. Hou, *J. Chem. Phys.*, 2008, **128**, 234705.
90 V. Iancu, A. Deshpande and S.-W. Hla, *Nano Lett.*, 2006, **6**, 820.
91 I. Fernández-Torrente, K. J. Franke and J. I. Pascual, *Phys. Rev. Lett.*, 2008, **101**, 217203.
92 C. Iacovita, M. V. Rastei, B. W. Heinrich, T. Brumme, J. Kortus, L. Limot and J. P. Bucher, *Phys. Rev. Lett.*, 2008, **101**, 116602.
93 G. P. Brivio and M. I. Trioni, *Rev. Mod. Phys.*, 1999, **71**, 231.
94 J. A. Stroscio and D. M. Eigler, *Science*, 1991, **254**, 1319.
95 P. Zeppenfeld, C. P. Lutz and D. M. Eigler, *Ultramicroscopy*, 1992, **42–44**, 128.
96 M.-L. Bocquet and P. Sautet, *Surf. Sci.*, 1996, **360**, 128.
97 L. Bartels, G. Meyer and K.-H. Rieder, *Appl. Phys. Lett.*, 1997, **71**, 213.
98 R. K. Tiwari, D. M. Otálvaro, C. Joachim and M. Saeys, *Surf. Sci.*, 2009, **603**, 3286.
99 J. Yoshinobu, M. Kawai, I. Imamura, F. Marumo, R. Suzuki, H. Ozaki, M. Aoki, S. Masuda and M. Aida, *Phys. Rev. Lett.*, 1997, **79**, 3942.
100 H. Q. Wang, C. G. Changgan, Q. X. Qunxiang, B. Wang, J. L. Yang, J. G. Hou and Q. S. Zhu, *Surf. Sci.*, 1999, **442**, L1024.
101 K. Sakamoto, M. Harada and D. Kondo, *Phys. Rev. B: Condens. Matter*, 1998, **58**, 13951.
102 C. Rogero, J. I. Pascual, J. Gómez-Herrero and A. M. Baró, *J. Chem. Phys.*, 2002, **116**, 832.
103 Á. J. Pérez-Jiménez, J. J. Palacios, E. Louis, E. SanFabián and J. A. Vergés, *ChemPhysChem*, 2003, **4**, 388.
104 C. Silien, N. A. Pradhan, W. Ho and P. A. Thiry, *Phys. Rev. B: Condens. Matter Mater. Phys.*, 2004, **69**, 115434.
105 M. K.-J. Johansson, A. J. Maxwell, S. M. Gray, P. A. Brühwiler, D. C. Mancini, L. S. O. Johansson and N. Mårtensson, *Phys. Rev. B: Condens. Matter*, 1996, **54**, 13472.
106 A. J. Maxwell, P. A. Brühwiler, S. Andersson, D. Arvanitis, B. Hernnäs, O. Karis, D. C. Mancini and N. Mårtensson, *Phys. Rev. B: Condens. Matter*, 1995, **52**, R5546.
107 N. Nilius, *Surf. Sci. Rep.*, 2009, **64**, 595.
108 T. L. Thompson and J. T. Yates, *Chem. Rev.*, 2006, **106**, 4428.
109 X. Chen and S. S. Mao, *Chem. Rev.*, 2007, **107**, 2891.
110 U. Diebold, *Surf. Sci. Rep.*, 2003, **48**, 53.
111 K. Onda, B. Li, J. Zhao, K. D. Jordan, J. L. Yang and H. Petek, *Science*, 2005, **308**, 1154.
112 T. Minato, Y. Sainoo, Y. Kim, H. S. Kato, K. Aika, M. Kawai, J. Zhao, H. Petek, T. Huang, W. He, B. Wang, Z. Wang, Y. Zhao, J. L. Yang and J. G. Hou, *J. Chem. Phys.*, 2009, **130**, 124502.
113 Y. Zhao, Z. Wang, X. F. Cui, T. Huang, B. Wang, Y. Luo, J. L. Yang and J. G. Hou, *J. Am. Chem. Soc.*, 2009, **131**, 7958.
114 W. Göpel, G. Rocker and R. Feierabend, *Phys. Rev. B*, 1983, **28**, 3427.

115 M. Menetrey, A. Markovits and C. Minot, *Surf. Sci.*, 2003, **524**, 49.
116 J. R. Hahn and W. Ho, *J. Chem. Phys.*, 2005, **122**, 244704.
117 M. Ohara, Y. Kim, S. Yanagisawa, Y. Morikawa and M. Kawai, *Phys. Rev. Lett.*, 2008, **100**, 136104.
118 H. Ueba and B. N. J. Persson, *Phys. Rev. B: Condens. Matter Mater. Phys.*, 2007, **75**, 041403(R).
119 H.-J. Shin, J. Jung, K. Motobayashi, S. Yanagisawa, Y. Morikawa, Y. Kim and M. Kawai, *Nat. Mater.*, 2010, **9**, 442.
120 C. J. Chen, *Introduction to Scanning Tunneling Microscopy*, Oxford University Press, 1993.
121 J. Bardeen, *Phys. Rev. Lett.*, 1961, **6**, 57.
122 B. Li, H. Q. Wang, J. L. Yang and J. G. Hou, *Ultramicroscopy*, 2004, **98**, 317.
123 J. R. Hahn and W. Ho, *Phys. Rev. Lett.*, 2001, **87**, 196102.
124 K. F. Kelly, D. Sarkar, S. Prato, J. S. Resh, G. D. Hale and N. J. Halas, *J. Vac. Sci. Technol., B*, 1996, **14**, 593.
125 Y. Xue, S. Datta, S. Hong, R. Reifenberger, J. I. Henderson and C. P. Kubiak, *Phys. Rev. B: Condens. Matter*, 1999, **59**, R7852.
126 P. Sutter, P. Zahl, E. Sutter and J. E. Bernard, *Phys. Rev. Lett.*, 2003, **90**, 166101.
127 W. Wulfhekel and J. Kirschner, *Annu. Rev. Mater. Res.*, 2007, **37**, 69.
128 L. Chen, Z. P. Hu, A. D. Zhao, B. Wang, Y. Luo, J. L. Yang and J. G. Hou, *Phys. Rev. Lett.*, 2007, **99**, 146803.
129 Z. P. Hu, L. Chen, A. D. Zhao, Z. Y. Li, B. Wang, J. L. Yang and J. G. Hou, *J. Phys. Chem. C*, 2008, **112**, 15603.
130 N. P. Guisinger, M. E. Greene, R. Basu, A. S. Baluch and M. C. Hersam, *Nano Lett.*, 2004, **4**, 55.
131 T. Rakshit, G.-C. Liang, A. W. Ghosh and S. Datta, *Nano Lett.*, 2004, **4**, 1803.
132 T. Rakshit, G.-C. Liang, A. W. Ghosh, M. C. Hersam and S. Datta, *Phys. Rev. B: Condens. Matter Mater. Phys.*, 2005, **72**, 125305.

